Introducing Dualem to the IUSS Working Group on Proximal Soil Sensing

R. Taylor
Dualem Inc., Milton, ON, L9T 3A2, Canada

Abstract

The DUALEM-4 was developed from 1995 to 1999 by our group experienced in airborne electromagnetics, seeking to implement the stability, sensitivity and robustness of airborne systems in practical and economical ground instruments. DUALEM instruments incorporate at-least-two arrays with significantly different depth-sensitivities. In 2004 we introduced the shallower-sensing DUALEM-1S to address applications in agriculture. Since then, a growing number of soil scientists are publishing results that make use of the data quality of an increasing variety of DUALEM instruments.

Keywords: electromagnetic induction, electrical conductivity, stability, phase

Technical Basis

The technology of DUALEM instruments is based on helicopter-borne electromagnetic (EM) systems that became sufficiently stable and sensitive to map (Fraser, 1978) and sound (Sengpiel, *et al*., 1981) conductivity by the 1980s. The preferred array in these systems for conductivity estimation has always been horizontal coplanar (HCP) due to its quality of in-phase signal. Precision at the parts-per-million (ppm) level in both in-phase and quadrature amplitude is necessary for quantitative interpretation of airborne data where conductivity decreases to a few millisiemens per metre (mS/m).

Ground clearance of 30-m is considered the minimum height for safe and smooth surveying with helicopter-borne systems. Proximal instruments, typically used within 1 m of the surface, receive much stronger signal. The enables quantitative interpretation of data with roughly an orders-of-magnitude less precision, as can be acquired with instruments of portable weight and size, and practical expense.

DUALEM instruments incorporate HCP arrays and perpendicular (PRP) arrays. The first EM instrument for measuring soil-conductivity (Howell, 1966) used a PRP array 1-m in length. The PRP array has excellent linearity between quadrature amplitude and true conductivity and, as implemented in DUALEM instruments, multi-year base-level stability of better than 1 mS/m.

Nomenclature

The numerical suffix hyphenated to the name of a DUALEM instrument indicates the length in metres of the incorporated arrays. For example, the DUALEM-1 incorporates a HCP and a PRP array, each with nominal length of 1 m. The longest instrument built at present, the DUALEM-642, incorporates (i) a 6-m HCP array, (ii) a 6.1-m PRP array, (iii) a 4-m HCP array, (iv) a 4.1-m PRP array, (v) a 2-m HCP array and (vi) a 2.1-m PRP array.

An S appended to the numbers indicates a sensor with the given arrays, but without the ancillary items that make a stand-alone instrument. For example, the DUALEM-1S is the sensor of the DUALEM-1 instrument. Sensors have monitors for pitch and roll, LED indicators of operational status and an internal logger for data and positioning. A sensor communicates in text through its serial port, with output in standard NMEA-format.

A DUALEM instrument contains a sensor with an internal WAAS-enabled GPS, a hand-held weatherproof display/keypad/battery-pack, and a harness with feet that clamp to the sensor. For example, Figure 1 shows the DUALEM-1 and sled that were used to map the demonstration site at the 2nd Global Proximal Soil Sensing Workshop in Montreal, May 18, 2011. (See discussion after References). The clamping feet are fixed with plastic bolts to the sled.

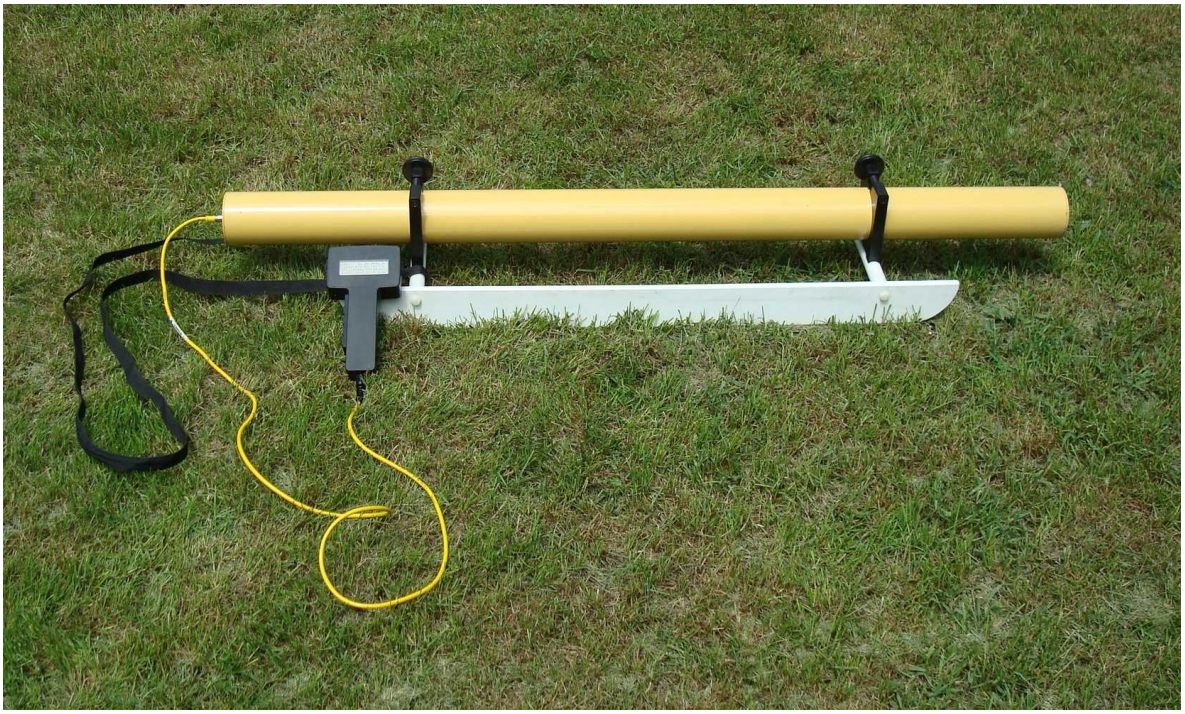

Figure 1: DUALEM-1 on sled.

Since the transmitter coil is separated from the dual receiver-coils by more-than-several coil diameters, the coils can be considered to be oscillating magnetic dipoles for the purpose of interpreting response. There is some currency among soil scientists for the term “vertical dipole” to describe the HCP array. We avoid this term when describing an array as it is ambiguous; it does not specify the arrangement of the dipoles. For example, vertical dipoles are also used in the coaxial system of the EM borehole-probe, and the vertical-dipole transmitter of a DUALEM sensor is integral to its PRP array(s).

Definitions

Induction number (IN) is a dimensionless parameter that characterizes EM response. IN is the ratio of array-length to the skin-depth of the EM field in the earth. At low-induction-number (LIN), quadrature amplitude is at least ten-times in-phase amplitude, and in-phase response can be ignored in the interpretation of apparent electrical conductivity (ECa). By an approximation (Wait, 1962) that can be made at LIN, ECa is linearly proportional to quadrature amplitude, depth sensitivity is a function only of array length, and ECa over a layered earth is sum of the conductivity of each layer by the cumulative sensitivity through the depth-interval of the layer. With few exceptions to the present, ECa in soil science has been interpreted linearly from quadrature amplitude using the LIN approximation.

Figure 2 shows the in-phase and quadrature responses of the HCP and PRP arrays (Wait, 1955) at low amplitude, along with the LIN boundary (defined as 10:1 quadrature-amplitude to in-phase-amplitude). The symbols on each response-curve show induction-number intervals of 0.1, *i.e*. the symbols show responses at induction numbers from 0 to 0.4.

The LIN boundary intersects the HCP curve at the induction number 0.092, and the PRP curve at the induction number 0.34. For the 9-kHz DUALEM operating frequency, these LIN limits correspond to 240 mS/m for the 1-m HCP array and 1700 mS/m for the 1.1-m PRP array of the DUALEM-1. As IN is proportional to array length and the square-root of conductivity, corresponding LIN limits of conductivity for other DUALEM arrays are 60 mS/m for 2-m HCP, 740 mS/m for 2.1-m PRP, 15 mS/m for 4-m HCP, 190 mS/m for 4.1-m PRP, 7 mS/m for 6-m HCP and 87 mS/m for 6.1-m PRP. Higher conductivities provide stronger responses but, above LIN, in-phase amplitude should be used in the interpretation of conductivity and sampled volume.

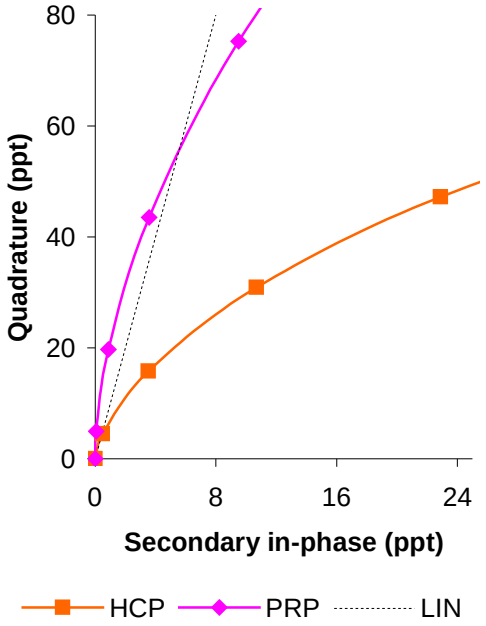

Figure 2: DUALEM arrays and LIN.

As increasing conductivity drives responses above LIN, the increasing in-phase amplitude should be used in order to avoid underestimating conductivity. Also, spatial sensitivity becomes a function of 3 dimensions, rather than simply of depth. The use of the full (in-phase and quadrature) EM response to interpret the conductivity of a 3-dimensional volume is called a full solution.

Figure 3 shows the LIN cumulative depth-sensitivities of the HCP and PRP arrays. The HCP array accumulates 50 % of its sensitivity to a depth equivalent to 0.87 array-lengths, which is usually referred to the effective depth of the array. The effective depth of the PRP array is 0.29 array-lengths. The depths for 70 % cumulative sensitivity, usually called depth of exploration, are 1.6 array-lengths for the HCP array and 0.49 array-lengths for the PRP array.

As responses from higher conductivities increasingly exceed LIN, quadrature depth-sensitivity decreases, but the depth of the volume associated with full EM response tends to increase.

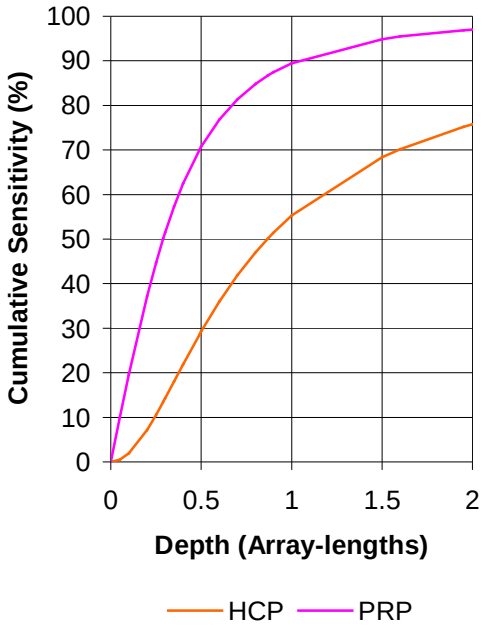

Figure 3: DUALEM depth sensitivities.

DUALEM in the Soil-Science Literature

Very brief descriptions follow of peer-reviewed papers with DUALEM results that relate to soil science. In rough chronological order, Allred, *et al*. (2005) mapped the artificial layers and structures of golf courses. Lee, *et al*. (2006) monitored ECa changes in fine-textured soil arising from a failed septic field. Eigenberg, *et al*. (2006) monitored soil and corn-crop status from 2000 to 2003. Abdu, *et al*. (2007) evaluated data accuracy at a resistive and a conductive site. Jiang, *et al*. (2007) investigated layering in claypan soils to estimate plant-available water capacity.

Gilley, *et al*. (2008) correlated ECa to wastes in runoff from feedlot surfaces, and mapped source locations. Urdanoz, *et al*. (2008) mapped a watershed to assess salinity and predict drain-water conductivity. Robinson, *et al*. (2008) imaged the links between watershed-scale patterns in soils and vegetation. Eigenberg, *et al*. (2008) monitored a vegetative area for treating feedlot runoff. Abdu, *et al*. (2008) predicted soil texture and water-holding capacity in a watershed.

Saey, *et al*. (2009) sounded the depth of clay beneath loess in Flanders. Robinson, *et al*. (2009) monitored soil-moisture dynamics in tropical deltaic soil around drainage and rainfall events. Simpson, *et al*. (2009) evaluated sensors for mapping anthropogenic soil disturbance. Jiang, *et al*. (2009) investigated the correlation between ECa and corn-yield in claypan soils. Woodbury, *et al*. (2009) estimated manure accumulation and spatial variability on a feedlot surface.

Santos, *et al*. (2010a) developed a laterally constrained LIN inversion algorithm, and tested it with data from sites of moderate to high conductivity. Santos, *et al*. (2010b) extended their laterally constrained inversion algorithm for full-solution, and tested it with data from sites of moderate to high conductivity. Singleton, *et al*. (2010) characterized ice-wedge polygons in arctic soils. Serrano, *et al*. (2010) mapped pasture variability as a basis for variable-rate fertilization. Zhu, *et al*. (2010a) mapped the depth and texture of soils. Simpson, *et al*. (2010) delineated Bronze Age ditches in coarse-to-medium soils. Sudduth, *et al*. (2010) sounded the depth of argillic soil beneath topsoil. Myers, *et al*. (2010) used proximal and penetrating sensors to map depth to claypan. Simpson, *et al*. (2010) mapped soil magnetic susceptibility. López-Lorzano, *et al*. (2010) delineated management units. Eigenberg, *et al*. (2010) evaluated precision management of waste and runoff in feedlots and treatment areas. Woodbury, *et al*. (2010) monitored soil-crop dynamics in a cornfield amended with manure. Mann, *et al*. (2010) investigated citrus-grove productivity. Robinson, *et al*. (2010) determined vegetation-soil relationships in a savanna. Zhu, *et al*. (2010b) evaluated data-interpolation in agricultural and forested terrain. Moffett, *et al*. (2010) studied salt-marsh salinity and vegetation zonation.

Saey, *et al*. (2011) imaged a clay paleolandscape beneath loess. Aragüés, *et al*. (2011) investigated soil, salinity, and irrigation at four sites around the Mediterranean. Urdanoz, *et al*. (2011) mapped pre- and post-irrigation salinity in a watershed, and its effect on drain-water salinity. De Smedt, *et al*. (2011) reconstructed paleochannel morphology in a sandy substrate. Santos, *et al*. (2011) mapped and sounded conductivity using full-solutions in a riverine plain of high conductivity. Triantafilis, *et al*. (2011) imaged a leachate plume in aeolian sand.

References

Abdu, H., Robinson, D.A. and Jones, S.B. 2007. Comparing bulk soil electrical conductivity determination using the DUALEM-1S and EM38-DD electromagnetic induction instruments. Soil Science Society of America Journal **71** 189-196.

Abdu, H., Robinson, D.A., Seyfried, M. and Jones, S.B. 2008. Geophysical imaging of watershed subsurface patterns and prediction of soil texture and water holding capacity. Water Resources Research **44** W00D18 (10 pp.).

Allred, B.J., Redman, J.D., McCoy, E.L. and Taylor, R.S. 2005. Golf Course Applications of Near-Surface Geophysical Methods: A Case Study. Journal of Environmental and Engineering Geophysics **10**(1) 1-19.

Aragüés, R., Urdanoz, V., Çetin, M., Kirda, C., Daghari, H, Ltifi, W., Lahlou, M. and Douaik, A. 2011. Soil salinity related to physical soil characteristics and irrigation management in four Mediterranean irrigation districts. Agricultural Water Management **98**(6) 959-966.

Fraser, D.C. 1978. Resistivity mapping with an airborne multicoil electromagnetic system. Geophysics **43**(1) 144-172.

De Smedt, P., Van Meirvenne, Meerschman, E., Saey, T., Bats, M., Court-Picon, M., De Reu, J., Zwertvaegher, A., Antrop, M., Bourgeois, J., De Maeyer, P., Finke, P.A., Verniers, J. and Crombé, P. 2011. Reconstructing paleochannel morphology with a mobile electromagnetic induction sensor. Geomorphology **130**(3-4) 136-141.

Eigenberg, R.A., Nienaber, J.A., Woodbury, B.L. and Ferguson, R.B. 2006. Soil conductivity as a measure of soil and crop status – A four-hear summary. Soil Science Society of America Journal **70** 1600-1611.

Eigenberg, R.A., Lesch, S.M., Woodbury, B. and Nienaber, J.A. 2008. Geospatial methods for monitoring a vegetative treatment area receiving beef feedlot runoff. Journal of Environmental Quality **37** S-68-S-77.

Eigenberg, R.A., Woodbury, B.L., Nienaber, J.A., Spiehs, M.J., Parker, D.B. and Varel, V.H. 2010. Conductivity and multiple linear regression for precision monitoring of beef feedlot manure and runoff. Journal of Environmental and Engineering Geophysics **15**(3) 175-184.

Gilley, J.E., Berry, E.D., Eigenberg, R.A., Marx, D.B. and Woodbury, B.L. 2008. Spatial variations in nutrient and microbial transport from feedlot surfaces. Transactions of the ASABE **51**(2) 675-684.

Howell, M.I. 1966. A soil conductivity meter. Archaeometry **9** 3-19.

Jiang, P., Anderson, S.H., Kitchen, N.R., Sudduth, K.A. and Sadler, E.J. 2007. Estimating plant-available water capacity for claypan landscapes using apparent electrical conductivity. Soil Science Society of America Journal **71** 1909-1908.

Jiang, P., He, Z., Kitchen, N.R. and Sudduth, K.A. 2009. Bayesian analysis of within-field variability of corn yield using a spatial hierarchical model. Precision Agriculture **10** 111-127.

Lee, B.D., Jenkinson, B.J., Doolittle, J.A., Taylor, R.S. and Tuttle, J.W. 2006. Electrical conductivity of a failed septic system soil absorption field. Vadose Zone Journal **5** 757-763.

López-Lozano, R., Casterad, M.A. and Herrero, J. 2010. Site-specific management units in a commercial maize plot delineated using very high resolution remote sensing and soil properties mapping. Computers and Electronics in Agriculture **73**(2) 219-229.

Mann, K.K., Schumann, A.W. and Obreza, T.A. 2011. Delineating productivity zones in a citrus grove using citrus production, tree growth and temporally stable soil data Precision Agriculture (Online First: 8 September 2010).

Moffett, S.B., Robinson, D.A. and Gorelick, S.M. 2010. Relationship of salt marsh vegetation zonation to spatial patterns in soil moisture, salinity and topography. Ecosystems **13** 1287-1302.

Myers, D.B., Kitchen, N.R., Sudduth, K.A., Grunwald, S., Miles, R.J., Sadler, E.J. and Udawatta, R.P. 2010. Combining proximal and penetrating soil electrical conductivity sensors for high-resolution digital soil mapping. Porgress in Soil Science **1**(4) 233-243.

Robinson, D.A., Abdu, H., Jones, S.B. Seyfried, M., Lebron, I. and Knight, R. 2008. Eco-geophysical imaging of watershed-scale soil patterns links with plant community spatial patters. Vadose Zone Journal **7**(4) 1132-1138.

Robinson, D.A., Lebron, I., Kocar, B., Phan, K., Sampson, M., Crook, N. and Fendorf, S. 2009. Time-lapse geophysical imaging of soil moisture dynamics in tropical deltaic soils: An aid to interpreting hydrological and geochemical processes. Water Resources Research **45** W00D32 (12 pp.).

Robinson, D.A., Lebron, I. and Querejeta, J.I. 2010. Determining soil-tree-grass relationships in a California oak savanna using eco-geophysics. Vadose Zone Jouranl **9**(3) 528-536.

Saey, T., Simpson, D., Vermeersch, H., Cockx, L. and Van Meirvenne, M. 2009. Comparing the EM38DD and DUALEM-21S sensors for depth-to-clay mapping. Soil Science Society of America Journal **73**(1) 7-12.

Saey, T., Van Meirvenne, M., De Smedt, P., Cockx, L., Meerschman, E., Islam, M.M. and Meeuws, F. 2011. Mapping depth-to-clay using fitted multiple depth response curves of a proximal EMI sensor. Geoderma **162**(1-2) 151-158.

Santos, F.A.M., Triantafilis, J., Burzgulis, K.E. and Roe, J.A.E. 2010a. Inversion of multiconfiguration electromagnetic (DUALEM-421) profiling data using a one-dimensional laterally constrained algorithm. Vadose Zone Journal **9** 117-125.

Santos, F.A.M., Triantafilis, J., Taylor, R.S., Holladay, S. and Burzgulis, K.E. 2010b. Inversion of conductivity profiles from EM using full-solution and a 1-D laterally constrained algorithm. Journal of Environmental and Engineering Geophysics **15**(3) 163-174.

Santos, F.A.M., Triantafilis, J. and Burzgulis, K.E. 2011. A spatially constrained 1D inversion algorithm for quasi-3D conductivity imaging: Application to DUALEM-421 data collected in a riverine plain. Geophysics **76**(2) 45-53.

Sengpiel, K.P. and Meiser, P. 1981. Locating the fresh water/salt water interface on Spiekeroog Island by airborne EM resistivity/depth mapping. *Geologisches Jahrbuch* **C 29**. Hannover.

Serrano, J.M., Peça, J.O., da Silva, J.R.M. and Shaidian, S. 2010. Mapping soil and pasture variability with an electromagnetic induction sensor. Computers and Electronics in Agriculture **73** 7-16.

Simpson, D., Van Meirvenne, M., Saey, T., Vermeersch, H., Bourgeois, J., Lehouck, A., Cockx, L., and Vitharana, U.W.A. 2009. Evaluating the multiple coil configurations of the EM38DD and DUALEM-21S sensors to detect archaeological anomalies. Archaeological Prospection 1**6** 91-102.

Simpson, D., Van Meirvenne, M., Lück, E., Bourgeois, J. and Rühlmann, J. 2010. Prospection of two circular Bronze Age ditches with multi-receiver electrical

conductivity sensors (North Belgium). Journal of Archaeological Science **37** 2198-2306.

Simpson, D., Van Meirvenne, M., Lück, E., Rühlmann, J., Saey, T. and Bourgeois, J. 2010. Sensitivity of multi-coil frequency domain electromagnetic induction sensors to map soil magnetic susceptibility. European Journal of Soil Science **61**(4) 469-478.

Singleton, A.C., Osinski, G.R., Samson, C., Williamson, M.-C. and Holladay, S. 2010. Electromagnetic characterization of polar ice-wedge polygons: Implications for periglacial studies on Mars and Earth. Planetary and Space Science **58** 472-81.

Sudduth, K.A., Kitchen, N.R., Myers, D.B. and Drummond, S.T. 2010. Mapping depth to agillic soil horizons using apparent electrical conductivity. Journal of Environmental and Engineering Geophysics **15**(3) 135-146.

Triantafilis, J., Roe, J.A.E. and Santos, F.A.M. 2011. Detecting a leachate plume in an aeolian sand landscape using a DUALEM-421 induction probe to measure electrical conductivity followed by inversion modelling. Soil Use and Management (in press).

Urdanoz, V., Anezkata, E., Claveria, I., Ochoa, V. and Aragüés, R. 2008. Mobile and georeferenced electromagnetic sensors and applications for salinity assessment. Spanish Journal of Agricultural Research **6**(3) 469-478.

Urdanoz, V. and Aragüés, R. 2011. Pre- and post-irrigation mapping of soil salinity with electromagnetic induction techniques and relationships with drainage water salinity. Soil Science Society of America Journal **75**(1) 207-215.

Wait, J.R. 1955. Mutual electromagnetic coupling of loops over a homogeneous ground. Geophysics **20** 630-637.

Wait, J.R. 1962. A note on the electromagnetic response of a stratified earth. Geophysics **27** 382-385.

Woodbury, B.L., Lesch, S.M., Eigenberg, R.A., Miller, D.N. and Spiehs, M.J. 2009. Electromagnetic induction sensor data to identify areas of manure accumulation on a feedlot surface. Soil Science Society of America Journal **73**(6) 2068-2077.

Woodbury, B.L., Eigenberg, R.A., Nienaber, J.A. and Spiehs, M.J. 2010. Soil-crop dynamic depth response determined from TDR of a corn silage field compared to EMI measurements. Journal of Environmental and Engineering Geophysics **15**(3) 185-196.

Zhu, Q., Lin, H. and Doolittle, J. 2010a. Repeated electromagnetic induction surveys for improved soil mapping in an agricultural landscape. Soil Science Society of America Journal **74**(5) 1763-1774.

Zhu, Q. and Lin, H.S. 2010. Comparing ordinary kriging and recession kriging for soil properties in contrasting landscapes. Pedosphere **20**(5) 594-606.

Demonstration Site Results

The DUALEM-1 on a sled, as shown in Figure 1, was pulled on a serpentine path to map the Workshop demonstration site at Macdonald campus of McGill University. Also, a vertical sounding was performed at a point near the northern edge of the site. The sounding entailed measuring ECa at several heights, to enable analysis of conductive layering.

Figure 4 shows the sounding measurements from the dual arrays at heights of roughly 0.1-, 0.5-, 1-, 1.6- and 2.1-m, and the response curves of a model that fit closely to the measurements.

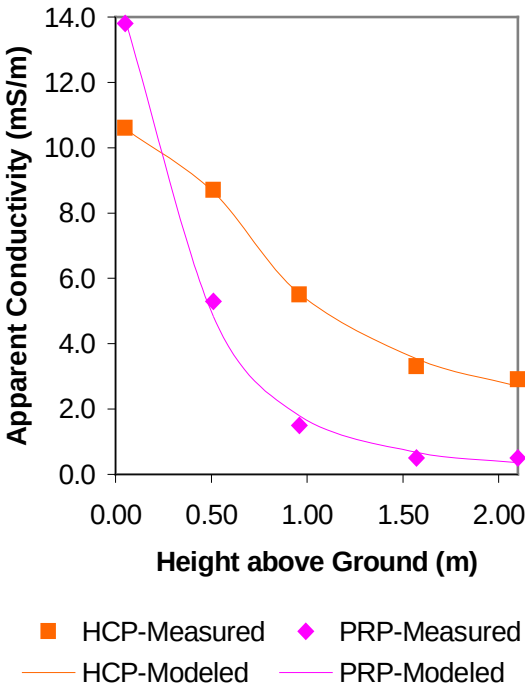

Figure 4: Model responses fitted to sounding measurements.

The model has 5 parameters, (i) surficial-layer thickness, (ii) surficial-layer conductivity, (iii) underlying conductivity, (iv) HCP offset and (v) PRP offset. Surficial-layer thickness was constrained to be no less than 0.2 m. An automated search-routine to minimize model-measurement discrepancy assigned this thickness, along with 28 mS/m as surficial-layer conductivity, 8 mS/m as underlying conductivity, 0.4 mS/m as HCP offset and –0.01 mS/m as PRP offset.

The maps that follow in Figure 5 show the data acquired along the serpentine traverse. Positioning of data was provided by the GPS receiver built into the sensor. WAAS-enabled GPS positional accuracy for eastings and northings is typically within a few metres, and for elevation is typically within a few tens of metres.

The map on the left plots elevation, and tight interpolation for contouring shows the survey path. The measurements were made at 1-s intervals, as the traverse proceeded at walking speed. Broader interpolation extends the contouring of the maps of PRP ECa, HCP ECa and HCP in-phase.

The dual maps of Ea have similar levels and patterns, but the 0.13-m surveying height of the sensor on the sled decreases the PRP values more. Thus, the ECa maps suggest that the material within the effective depth of the PRP array is generally more conductive than the underlying material, as was concluded from the sounding analysis.

The feature in the south-eastern corner of the maps has response that is beyond the contouring of the PRP ECa map, and beyond both the contouring and color scale of the HCP maps. A response of this amplitude, in both ECa and in-phase, likely is due to buried metal. The in-phase map also shows that the magnetic susceptibility of the shallow soil grades from higher in the southeast to lower in the northwest.

McGill PSS Workshop Site: Elevation and Electromagnetic Maps

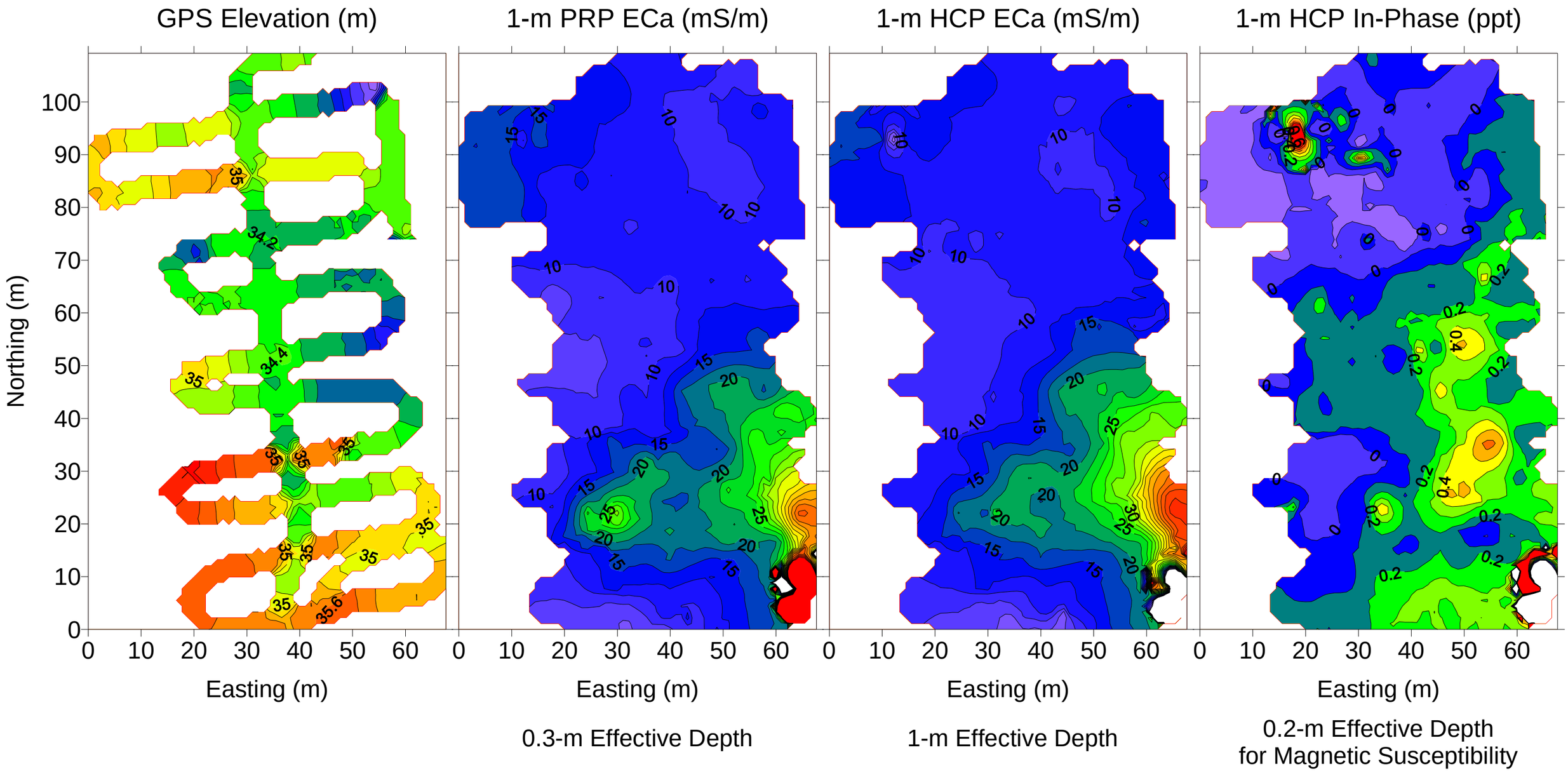

(Effective Depth is depth to 50-% cumulative sensitivity for conductivity or susceptibility. Data acquired 2011-5-18.)

Figure 5: Maps from DUALEM-1 positioning and measurements.